

NUREG-0259
NRC-7

A LOOK AT ALTERNATE CORE DISRUPTION ACCIDENTS IN LMFBRs

C. K. Chan*, T. K. Min, and D. Okrent*

***Under National Science Foundation Grant OEP75-20318**

Principal Investigators

I. Catton

W. E. Kastenber

Manuscript Completed: April 1977

Date Published: May 1977

School of Engineering and Applied Science

University of California

Los Angeles, CA 90024

Prepared for

**Division of Reactor Safety Research
Office of Nuclear Regulatory Research**

U. S. Nuclear Regulatory Commission

Under Contract No. AT(49-24)-0246

ra



BIBLIOGRAPHIC DATA SHEET	1. Report No. NUREG-0259	2.	3. Recipient's Accession No.
	4. Title and Subtitle A Look At Alternate Core Disruption Accidents in LMFBRs		5. Report Date June 1977
7. Author(s) C.K. Chan, T.K. Min and D. Okrent	8. Performing Organization Rept. No.		6.
9. Performing Organization Name and Address School of Engineering and Applied Science University of California at Los Angeles Los Angeles, CA 90024		10. Project/Task/Work Unit No.	11. Contract/Grant No. AT(49-24)-0246
12. Sponsoring Organization Name and Address Division of Reactor Safety Research Office of Nuclear Regulatory Research U.S. Nuclear Regulatory Commission Washington, D.C. 20555		13. Type of Report & Period Covered Topical Report	14.
15. Supplementary Notes			
16. Abstracts This report explores in preliminary fashion the course of a postulated accident scenario in an LMFBR involving rupture of all piping connected to the reactor vessel in the event of an earthquake (or an equivalent scenario involving both loss of heat removal and system rupture). The core is successfully shut down but decay heat imposes a threat to core integrity.			
17. Key Words and Document Analysis. 17a. Descriptors			
17b. Identifiers/Open-Ended Terms			
17c. COSATI Field/Group			
18. Availability Statement Release Unlimited		19. Security Class (This Report) UNCLASSIFIED	21. No. of Pages 64
		20. Security Class (This Page) UNCLASSIFIED	22. Price PCA04-A01

PREFACE

This report represents one aspect of the research program "Safety Considerations of Commercial Liquid Metal Fast Breeder Reactors" (AT(04-3) PA223 and AT(49-24)-0246) funded by the U.S. Nuclear Regulatory Commission, Division of Reactor Safety Research. The research program is divided into the following tasks: a) transient analysis of fuel elements, b) accident analysis, c) post accident heat removal, d) fuel-coolant interactions and e) thermodynamic effects.

Reports prepared previously under this grant include the following:

1. Post Accident Heat Removal with Advanced LMFBR Fuels, R. D. Gasser, UCLA-ENG-7518 (March 1975).
2. Dry-Out of a Fluidized Particle Bed with Internal Heat Generation, R. S. Keowen and I. Catton, UCLA-ENG-7519 (March 1975).
3. Laminar Natural Convection from Blunt Bodies with Arbitrary Surface Heat Flux or Surface Temperature, G. M. Harpole, UCLA-ENG-7527 (April 1975).
4. Preliminary Assessments of Carbide Fuel Pins During Mild Overpower Transients, G. M. Nickerson, UCLA-ENG-7582 (October 1975).
5. A Simplified Method of Computing Clad and Fuel Strain and Stress During Irradiation, Y. Sun and D. Okrent, UCLA-ENG-7591 (Part I) (October 1975).
6. An Experimental Study of the Thermal Interaction for Molten Tin Dropped into Water, V. M. Arakeri, I. Catton, W. E. Kastenbergl and M. S. Plesset, UCLA-ENG-7592 (December 1975).

7. A Mechanistic Study of Fuel Freezing and Channel Plugging During Fast Reactor Overpower Excursions, V. K. Dhir, K. Wong and W. E. Kastenberg, UCLA-ENG-7679 (July 1976).
8. A Simulation of Thermal Phenomenon Expected in Fuel Coolant Interactions in LMFBR's, J. Yasin, UCLA-ENG-76100 (September 1976).
9. On the Nonequilibrium Behavior of Fission Gas Bubbles with Emphasis on the Effects of Equation of State, W. G. Steele, UCLA-ENG-76118 (December 1976).
10. A Method for the Determination of the Equation of State of Advanced Fuels Based on the Properties of Normal Fluids, M. J. Hecht, UCLA-ENG-76112 (December 1976).
11. A Simplified Method of Computing Clad and Fuel Strain and Stress During Irradiation, Y. Sun and D. Okrent, UCLA-ENG-7705 (Part II) (January 1977).
12. Natural Convection in Horizontal Fluid Layers, A. J. Suo-Anttila and I. Catton, UCLA-ENG-7706 (January 1977).
13. An Experimental Study of the Molten Glass/Water Thermal Interaction Under Free and Forced Conditions, V. H. Arakeri, I. Catton, and W. E. Kastenberg, UCLA-ENG-7714, (January 1977).
14. Study of Dryout Heat Fluxes in Beds of Inductively Heated Particles, V. K. Dhir and I. Catton, UCLA-ENG-7725, (February 1977).

SUMMARY

This report explores in preliminary fashion the course of a postulated accident scenario in an LMFBR involving rupture of all piping connected to the reactor vessel in the event of an earthquake (or an equivalent scenario involving both loss of heat removal and system rupture). The core is successfully shut down but decay heat imposes a threat to core integrity.

In the event of a sudden rupture of all piping attached to the reactor vessel, the coolant level in the vessel drops to the level of the break location. Because of continuous decay heat production, natural circulation is maintained between the inlet and outlet plena. Using a simple hydraulic flow circuit together with a transient heat conduction model, the natural circulation rate, and the temperature variations in the fuel, the cladding, and the coolant can then be calculated. It is found that the fuel temperature experiences a decrease as the power level decays while the cladding temperature increases to a maximum value of about 1,600° F before it follows the same trend as the fuel temperature. For the conditions assumed, it takes 5.6 hours for the cladding to reach the incipient boiling temperature. When bubbles are nucleated, the heat transfer at the cladding surface is improved. Both the fuel and the clad experience a temperature drop before they reach a quasi-steady state during nucleate boiling when evaporation of the sodium in the outlet plenum is taking place. It takes 32 hours for complete evaporation of all the sodium liquid in the upper plenum.

As the sodium level recedes in the core region, both the fuel and the cladding in the upper part of the core experience a rapid temperature rise. Taking into account the effects of axial power distribution and

axial heat conduction, clad melting is found to occur at a location close to the top of the core, and at a rate of $0.08 \text{ ft}^3/\text{sec}$. The sodium vapor velocity is not high enough to carry the molten steel to the upper blanket region. The molten steel is hence expected to move downward and plug the flow channels in the lower axial blanket region.

At the time of clad melt, the fuel experiences a temperature rise of approximately 2° F/sec while the temperature rise rate at the can wall is 10° F/sec , which is mainly caused by heat radiation from the fuel pin to the wall. Failure of the can wall may mark the start of gross fuel motion wherein fuel pellets can be arranged into a more compact geometry before they start to melt. Indeed, depending on the assumption of the fuel pellet arrangement and the distribution of the control rod material, the preliminary calculation indicates the possibility of the core gaining recriticality prior to much fuel melting. A detailed description of fuel behavior under nearly isothermal conditions prior to melting requires further study, as does the subsequent course of events in this postulated scenario.

TABLE OF CONTENTS

	<u>Page</u>
PREFACE	i
SUMMARY	iii
LIST OF FIGURES	vi
LIST OF TABLES	vii
LIST OF SYMBOLS	viii
1. INTRODUCTION	1
1.1 Background	1
1.2 System Analysis	2
1.3 Organization of the Report	2
2. ANALYTICAL METHODOLOGY	5
2.1 Introduction	5
2.2 Natural Circulation	7
2.3 Sodium Boiling	12
2.4 Core Dryout	14
2.5 Subassembly Failure Mode	19
3. RESULTS	21
4. CONCLUDING REMARKS	43
5. REFERENCES	45
APPENDIX A	47
APPENDIX B	51

LIST OF FIGURES

		<u>Page</u>
Figure 1.1.	General Configuration of the Heat Transport System, One of Three Loops.	3
Figure 2.1.	Natural Circulation Flow Model.	6
Figure 2.2.	Physical Model of the Core Dryout Process. . .	15
Figure 3.1.	Temperature Response during Natural Circulation and Boiling Periods.	22
Figure 3.2.	Standard Fission-Product Decay Heat Curve. . .	23
Figure 3.3.	Heat Transfer Coefficient and Circulation Rate.	30
Figure 3.4.	Axial Cladding and Fuel Temperatures during Core Dryout.	33
Figure 3.5.	Receding Speed of Liquid Sodium (U_f) and Sodium Vapor Velocity (U_g).	34
Figure 3.6.	Sodium Vapor Heat Transfer Coefficient.	35
Figure 3.7.	Fuel Rod Schematic for CRBRP Design.	37
Figure 3.8.	Fuel Assembly Schematic for CRBRP Design. . . .	38
Figure A.1.	Hydraulic Flow Resistance Circuit Diagram. . .	48
Figure A.2.	Simplified Hydraulic Circuit for Natural Convection.	49
Figure B.1.	Average Fuel Pin Temperatures after Clad Melt. .	52

LIST OF TABLES

		<u>Page</u>
Table 3.1.	Physical Parameters for CRBR Design.	24
Table 3.2.	Thermophysical Properties of Materials.	28
Table 3.3.	Heat Balance Table.	31
Table 3.4.	Properties of Fuel and Cladding Materials.	39
Table 3.5.	Results of Recritical Calculation.	41

LIST OF SYMBOLS

A	Area
\bar{A}	Cross section area
B	Radiosity
B_1, B_2, B_3	Constants defined by Equations (2.4), (2.5) and (2.6)
C_p	Specific heat
d	Droplet size
D_d	Bubble departure diameter
f	Bubble departure frequency
F	View factor
g	Gravitational constant
Gr	Grashoff number
h	Heat transfer coefficient
h_{fg}	Latent heat of evaporation
h_{sf}	Heat of fusion
H	Irradiation
k	Thermal conductivity
K	Fluid resistance
K_{TOT}	Total fluid resistance
ℓ	Sodium level
L	Core length
L_c	Loop length
L_1	Distance between lower and upper plena
M	Mass
\bar{M}	Molecular weight
\dot{M}	Mass flow rate
n	Number of fuel elements

LIST OF SYMBOLS (Continued)

P	Perimeter
Pr	Prandtl number
q''	Decay heat
Q	Heat flux
R	Gas constant
R_1	Thermal resistance from fuel to clad
R_2	Thermal resistance from clad to coolant
t	Time
T	Temperature
u	Velocity
u_l	Liquid velocity
V	Volume
α	Thermal diffusivity
β	Sodium expansion coefficient
ΔP	Pressure drop
ϵ	Emissivity
η	Number of fuel elements
μ	Viscosity
ν	Kinematic viscosity
ρ	Density
σ	Surface tension
$\bar{\sigma}$	Stefan Boltzmann Constant

Subscripts

c	Sodium coolant
co	Core

LIST OF SYMBOLS (Continued)

Subscripts (Continued)

ϕ	Cladding
f	Fuel
g	Gap
i	Inlet plenum
L	Lower plenum
m	Melting
NB	Nucleate boiling
o	Outlet
s.s.	Stainless steel
u	Upper plenum
w	Can wall

1. INTRODUCTION

1.1 Background

One of the generic safety concerns in Fast Breeder Reactors is that the fuel is not arrayed in its most reactive configuration. Should there be ways of arranging this fuel in a more reactive configuration, it is possible to imagine recriticality which would subsequently lead to pressure driven disassembly. The currently analysed sequences leading to a recritical configuration usually involve the unprotected Loss of Flow Accident (LOF) or the Transient Overpower (TOP). While these two accident sequences could lead to rapid fuel melting and core disruption, the recriticality potential of the system may ultimately depend on the nature of the fuel distribution in the molten pool. In the so-called 'transition phase' of core disruption, it has been suggested by several authors [1,2] that some fuel and/or steel will be removed from the core region and frozen near the axial core boundaries in a large number of subassemblies, thus blocking further material removal. It has been estimated that material remaining in the disrupted core region will be dispersed by steel or fuel vapor formation. This boil-up phenomenon is estimated to occur at decay heat levels of about 10% nominal power [1]. However, it should be noted that this assessment depends to a large extent on the thermal and the hydrodynamic conditions of the molten core which are not yet completely understood [3].

On the other hand, one should realize that core disruption is not, in principle, limited to these two accident scenarios. One objective of this report is to examine another sequence, having a rather different time history, in which recriticality might occur. While a mechanistic approach is adopted here to follow the sequence of events of a postulated

accident initiated by a simultaneous break of both cold and hot legs in a looped type LMFBR, an attempt has been made to make the approach generic, so that it can be applied to similar accident scenarios. The present analysis does not carry the postulated accident to completion; rather, it examines the first phases and brings the event to the point where recriticality might occur.

1.2 System Analysis

Sodium-cooled, fast power reactor designs may be pool type or loop type [4]. The U.S. LMFBR program is sharply focused on the development of the loop type, as exemplified by the designs of the Fast Flux Test Facility (FFTF) [5], and Clinch River Breeder Reactor (CRBR) [6].

The CRBRP has a loop type heat transport system (Figure 1.1). A sudden rupture of all the vessel inlet and outlet piping would seriously affect the cooling of the core. Even after the core is successfully scrammed, the decay heat still imposes a potential threat to the core integrity. It is logical to deduce that the core is initially cooled by natural convection until the sodium reaches its boiling point. Then the reactor vessel begins to lose its coolant inventory. Eventually, the core is uncovered and this speeds up the fuel-temperature excursion. Because of its fairly low heating value, the decay heat power may lead to a different core disruption sequence in comparison with the situation induced by unprotected LOF or TOP.

1.3 Organization of the Report

This report is divided into five chapters. Following this introductory chapter is the detailed outline of the analytical method

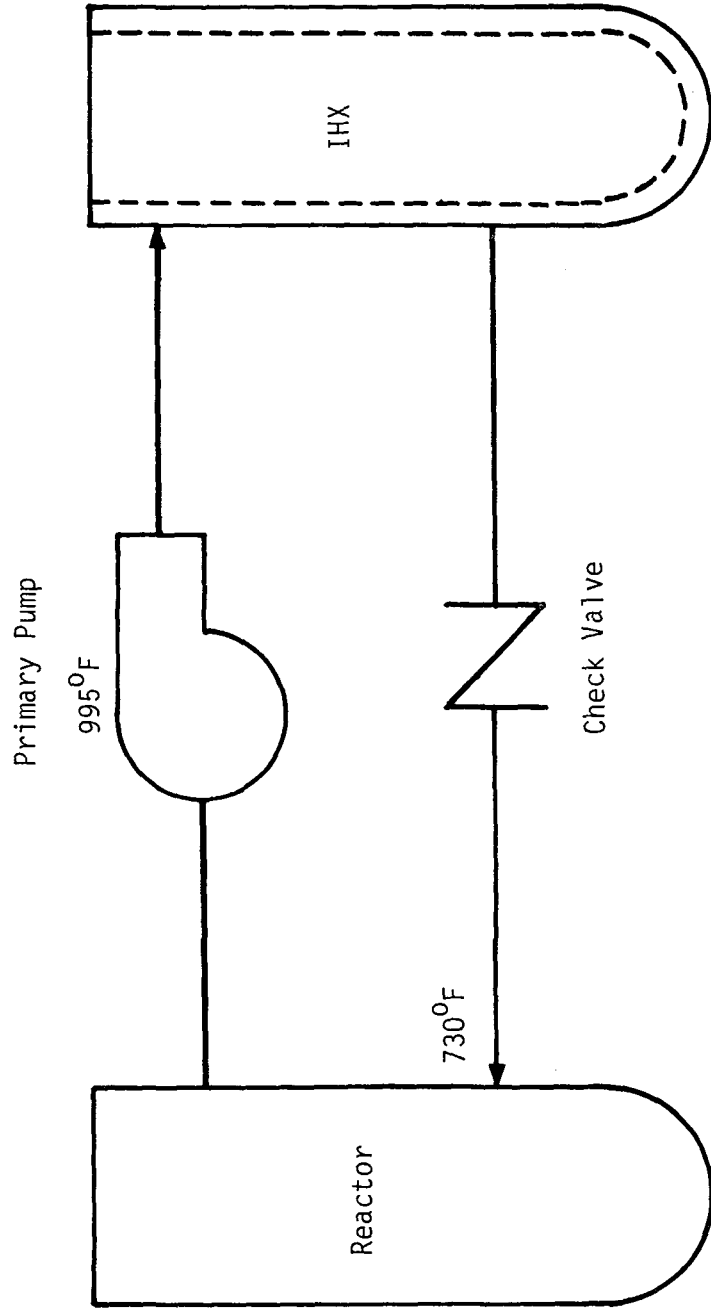


Figure 1.1 General Configuration of the Heat Transport System , One of Three Loops

that is used to evaluate the system response, in the event of a loss of the piping integrity (LPI). In the analytical model, a compromise is made between simplicity and accuracy, in order to bring out the significant physics of the problem. Numerical data are computed and presented in Chapter 3 where the design data of the CRBRP are chosen for the calculation. Discussion of the results and the concluding remarks of this preliminary study can be found in Chapter 4. Chapter 5 lists the references while two appendices are included to document the details of the technical information used in connection with the study.

2. ANALYTICAL METHODOLOGY

2.1 Introduction

In the event of a sudden rupture of all the piping attached to the reactor vessel, the coolant level in the vessel drops to the level of the break location. The scram action of the core would decrease the core power to the decay heat level. Because of this continuous heat production, a natural circulation is maintained between the lower and the upper plenum as shown in Figure 2.1. Depending on the heat transfer characteristic of the fuel rods, the cladding can be cooled by the circulating sodium stream. Local subcooled boiling will occur when the cladding reaches the incipient temperature of sodium boiling. During this subcooled boiling period, the vapor is rapidly condensed by the sodium liquid and so there is no net loss of sodium from the reactor vessel. When the sodium reaches the saturation temperature, bulk generation of the vapor takes place, and the sodium level starts to recede. Depending on the bubble cluster formation, cooling of the cladding can still be maintained if local liquid dryout is not prolonged. This two-phase flow regime, especially in the confined fuel bundle geometry, is still an unexplored research area. A simple model based on two-phase pressure drop and bubble generation frequency is adopted here as a first order estimation.

When the sodium starts to recede in the core, the upper part of the fuel rod is cooled by the sodium vapor, while the lower part is submerged in liquid sodium. At this stage, the axial heat generation profile in the fuel and the axial heat conduction may play an important role on the location of the clad failure. Fuel swelling is a possible

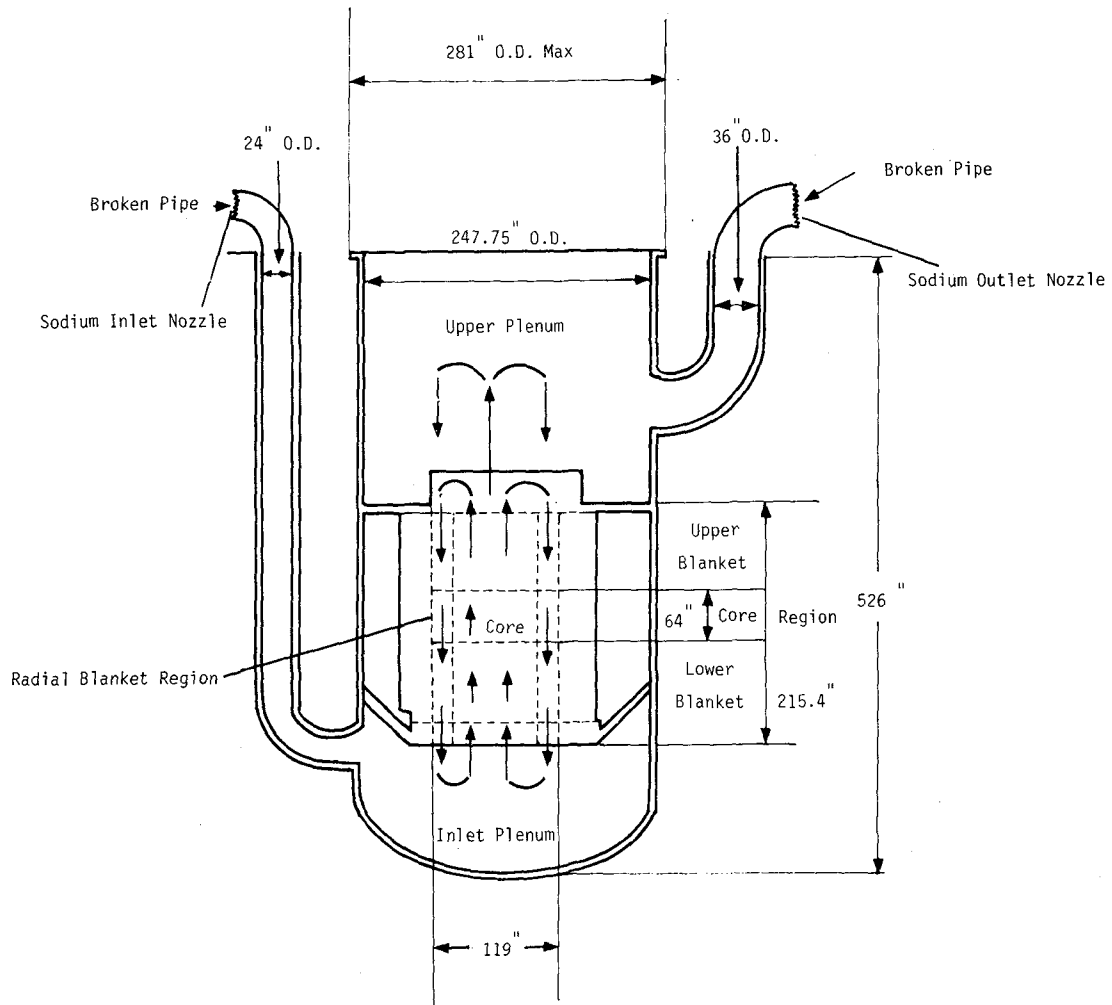


Figure 2.1. Natural Circulation Flow Model.

event. In case of clad melting, it is important to note where the molten steel will be dispersed. This depends on the sodium vapor velocity. If the clad melts before the fuel fails, the next state would be the propagation of the subassembly can wall failure.

In estimating the failure propagation rate of the fuel subassembly, the radial power distribution of the core cannot be ignored. If the subassembly is depleted of sodium, the major contributor for the can wall failure would be the heat radiated from the heated fuel pins. If the can failure rate is faster than fuel melting, recriticality can occur as result of fuel collapse. In the recriticality calculation, the location and the distribution of the control rod material have to be considered.

Only a few criticality calculations, using simple hand calculations, are performed in this study as a scoping effort of the accident sequential event.

2.2 Natural Circulation

As a compromise between simplicity and accuracy, the reactor is represented by three axial regions: the inlet plenum, the core and the outlet plenum. The core is represented by an average channel in which the fuel rod is surrounded by the sodium coolant. The natural circulation path is established as the hot sodium rises in the core and is replaced by the cold sodium from the lower plenum. The flow path is completed with the sodium flowing from the upper to the lower plenum region through the blanket as shown in Figure 2.1.

As the sodium is circulated, the temperature changes in the upper and the lower plenum (T_u and T_L) are obtained by an energy

balance which includes the heat absorbed by the steel structure as,

$$\left[(M_u C_p)_c + (M_u C_p)_{s.s.} \right] \frac{dT_u}{dt} = \dot{M}_{pc} (T_o - T_u) \quad (2.1)$$

$$\left[(M_L C_p)_c + (M_L C_p)_{s.s.} \right] \frac{dT_L}{dt} = \dot{M}_{pc} (T_u - T_L) \quad (2.2)$$

where $(M_u C_p)_{s.s.}$ and $(M_L C_p)_{s.s.}$ are the total heat capacity of the steel structure, $(M_u)_c$ and $(M_L)_c$ are the sodium mass inventories, in the upper and the lower plena, respectively.

$(C_p)_c$ is the specific heat of the sodium liquid

\dot{M} is the natural circulation rate and it is given by*

$$B_1 \dot{M}^3 + B_2 \dot{M}^2 - B_3 = 0 \quad (2.3)$$

where

$$B_1 = 2C_{pc} K_{TOT} \quad (2.4)$$

$$B_2 = h_c A_\phi K_{TOT} \quad (2.5)$$

$$B_3 = 4\beta g L_p^2 h_c A_\phi (T_\phi - T_i) \quad (2.6)$$

In these equations

K_{TOT} = overall hydraulic resistance in the flow path

h_c = the natural heat transfer coefficient. For a fuel bundle,

it is given by [7].

$$h_c = \frac{k_c}{L} (0.747(GrPr^2)^{0.147}) \quad (2.7)$$

where

Pr = Prandtl number

Gr = Grashoff number

k_c = sodium thermal conductivity

* The derivation of this equation is given in Appendix A.

β = volumetric sodium expansion coefficient

ρ_c = sodium density

L = core length

T_i = core inlet coolant temperature

A_ϕ = heat transfer area of the cladding

T_o = core outlet coolant temperature

T_ϕ = cladding temperature

The temperature distribution in the core is divided into three regions: the fuel, the cladding and the coolant. Inside the fuel, heat is generated as a result of the decay heat. Hence, by simple energy balance, these temperatures are given by:

$$(MC_p)_f \frac{dT_f}{dt} = q'''(t)V_f - \frac{1}{R_1} [T_f - T_\phi] \quad (2.8)$$

$$(MC_p)_\phi \frac{dT_\phi}{dt} = \frac{1}{R_1} [T_f - T_\phi] - \frac{1}{R_2} [T_\phi - T_c] \quad (2.9)$$

$$(MC_p)_c \frac{dT_c}{dt} = \frac{1}{R_2} [T_\phi - T_c] \quad (2.10)$$

where

$(MC_p)_f$, $(MC_p)_\phi$, $(MC_p)_c$ = Total heat capacity of the fuel element, cladding, and coolant, respectively

R_1 = Total thermal resistance of the fuel and the gap conductance,

$$\text{i.e. } R_1 = \frac{1}{4\pi k_f L \eta} + \frac{1}{h_g A_g}$$

where k_f = thermal conductivity of the fuel

L = height of the fuel element

η = total number of fuel elements in the core

h_g = gap conductance

A_g = total fuel surface area

R_2 = thermal resistance of sodium coolant film ($= \frac{1}{h_c A_\phi}$)

$q'''(t)$ = decay heat power

V_f = fuel volume

The coolant temperature is assumed to be the average of the core inlet and the core outlet temperatures, i.e.

$$T_c = \frac{T_o + T_i}{2} \quad (2.11)$$

An additional relation between T_o and T_i is obtained by balancing the total energy of the coolant channel, i.e.

$$h_c A_\phi (T_o - T_c) = \dot{M} C_{pc} (T_o - T_i) \quad (2.12)$$

Equations (2.1) to (2.12) constitute the basic equations for the evaluation of the fuel and the cladding temperature, the sodium temperatures in the core, in the upper and lower plenum, and in addition, the natural recirculation rate through the system. This natural circulation is assumed to prevail until the cladding reaches the temperature limit when surface boiling starts. This temperature limit is obtained by balancing the heat fluxes of the natural convection and the nucleate boiling regimes, i.e.

$$0.14 k_c \left[\left(\frac{\beta g}{\nu_c} \right) Pr_c \right]^{1/3} \Delta T_{SAT}^{4/3} = 0.0015 \rho_v h_{fg} \left[\frac{\alpha_c}{\pi} \right]^{1/2} \times$$

$$\left[\frac{2\sigma g}{\rho_c} \left(\frac{h_{fg} \bar{M} \rho_c}{2RT_{SAT}^2 \sigma} \right)^3 \right]^{1/4} \times$$

$$\left[\frac{\rho_c}{\mu_c} \left(\frac{k_c}{\rho_v h_{fg}} \right)^2 \left(\frac{\pi}{\alpha_c} \right) \right]^{5/8} (Pr_c)^{1/3} \times \Delta T_{SAT}^2 \quad (2.13)$$

The boiling heat flux is obtained from the Zuber correlation.

The symbols in equation (2.13) are

ρ_c for density;

h_{fg} for latent heat of vaporization;

α for thermal diffusivity;

σ for surface tension;

\bar{M} for molecular weight;

R for gas constant;

μ for viscosity ;

ν for kinematic viscosity ;

T_{SAT} for saturation temperature of sodium at 1 atmosphere.

The subscript c denotes the liquid phase, v stands for the vapor phase. $(\Delta T)_{SAT}$ represents the superheat temperature when sodium boiling occurs.

Since the channel coolant may not reach the saturation temperature when surface boiling occurs, the period following the first natural convection period is characterized by local subcooled boiling. Vapor is generated on the cladding surface but is rapidly condensed by either the coolant in the core or in the upper plenum. There is no net loss of vapor from the system. A check on the heat flux is necessary to ensure that the surface heat flux has not reached the critical value.

The governing equations for the temperatures are the same as the natural convection case except the heat transfer coefficient has to be modified to accommodate the boiling phenomenon. A brief literature survey reveals a basic lack of sodium boiling data. The Zuber correlation is chosen because it is better correlated with liquid metal data.

$$h_{NB} = 0.0015 \rho_V h_{fg} \left(\frac{\alpha_c}{\pi} \right)^{1/2} \left(\frac{2\sigma g_c}{\rho_c} \left(\frac{h_{fg} \bar{M} \rho_c}{2RT_{SAT}^2 \sigma} \right)^3 \right)^{1/4}$$

$$\left(\frac{\rho_c}{\mu_c} \left(\frac{k_c}{\rho_V h_{fg}} \right)^2 \left(\frac{\pi}{\alpha_c} \right) \right)^{5/8} (Pr)_c^{1/3} \Delta T_{SAT} \quad (2.14)$$

where the symbols are the same as in equation (2.13).

This subcooled boiling period is assumed to be terminated when the coolant in the upper plenum reaches the saturation temperature. At that time, the accident sequence steps into the third period.

2.3 Sodium Boiling

When bulk boiling occurs, the main driving force for circulation is no longer due to the temperature gradient. Instead, the buoyancy force of the vapor becomes the main driving force. The presence of the vapor in the flow path increases the flow resistance. The governing equations for the cladding and the fuel are the same as in the previous two periods. However, the momentum equation for the flow has to be modified to incorporate the two phase pressure drop as:

$$L_c \frac{d\dot{M}}{dt} = \rho_c g \delta V - g (\Delta P)_{co} A_{co} - g (\Delta P)_r A_r \quad (2.15)$$

where

L_c is the characteristic length for the flow circuit

$$\delta V = \frac{\dot{M}_V}{\rho_V} \text{ is the vapor volume} \quad (2.16)$$

$$\dot{M}_V = \frac{h_{NB} A_c (T_c - T_c)}{h_{fg}} \quad (2.17)$$

$$f = \frac{0.59}{D_d} \left(\frac{\sigma g (\rho_c - \rho_v)}{\rho_c^2} \right)^{1/4} \text{ is the frequency of bubble departure [8]} \quad (2.18)$$

$$D_d = 0.0208 \theta \left[\frac{\sigma}{g (\rho_c - \rho_v)} \right]^{1/2} \text{ is the diameter of the departing bubble [8]} \quad (2.19)$$

θ is the contact angle at the wall

A_{co} is the flow area in the core

A_r is the flow area in the blanket

The two phase pressure drop $(\Delta P)_{co}$ between the lower and the upper plenum is

$$(\Delta P)_{co} = (\overline{\Delta P})_{co} \left(\frac{h_{NB}^P}{2h_{fg}} \frac{P}{\dot{M}} \right) \left(\frac{\rho_c}{\rho_v} - 1 \right) (L^2 - Z_{SAT}^2) + (L_1 - L) \chi_Q \left(\frac{\rho_c}{\rho_v} - 1 \right) + L_1 \quad (2.20)$$

where

$(\overline{\Delta P})_{co}$ is the single phase pressure drop quality of sodium at core melt

$$\chi_Q = \frac{h_{NB}^P (T_\phi - T_c) (L - Z_{SAT})}{h_{fg} \dot{M}} \quad (2.21)$$

$$Z_{SAT} = \frac{\dot{M} (h_{SAT} - h_{in})}{(T_\phi - T_c) h_{NB}^P} \text{ distance from the bottom of the core where boiling starts} \quad (2.22)$$

L = core length

L_1 = distance between the location of inlet sodium saturation point and upper plenum

P = wetted perimeter

h_{SAT} = saturation enthalpy

h_{in} = inlet enthalpy

The system starts to lose the sodium coolant in the form of the vapor. The change of mass in the upper plenum is given by

$$\frac{dM_u}{dt} = -\frac{h_{NB} A_\phi}{h_{fg}} (T_\phi - T_c) \quad (2.23)$$

while the change in the lower plenum temperature is given by

$$\frac{dT_L}{dt} = \frac{(\dot{M}_L C_p)_c}{(\dot{M}_L C_p)_c + (\dot{M}_L C_p)_{s.s.}} (T_{SAT} - T_L) \quad (2.24)$$

This bulk boiling period is assumed to be terminated once the coolant level reaches to the top of the core.

2.4 Core Dryout

When the sodium level reaches to the top of the core, the core region can no longer be modeled as a single volume. Because of the continuous vapor loss of sodium, the sodium level in the core recedes leaving the upper part of the core cooled by sodium vapor only. Both the fuel and the cladding temperature will experience axial variation. The axial power distribution of the core must be considered in the estimation of the clad failure. If the core is modeled as shown in Figure 2-2, the fuel temperature distribution is given as

$$(\rho C_p)_f \bar{A}_f \frac{\partial T_f}{\partial t} = K_f \bar{A}_f \frac{\partial^2 T_f}{\partial x^2} + q'''(x,t) \bar{A}_f - \frac{1}{R_1} [T_f(x,t) - T_\phi(x,t)] \quad (2.25)$$

where $(\rho C_p)_f$ = heat capacity per unit volume of the fuel

T_f = fuel temperature

T_ϕ = clad temperature

\bar{A}_f = total fuel cross-sectional area

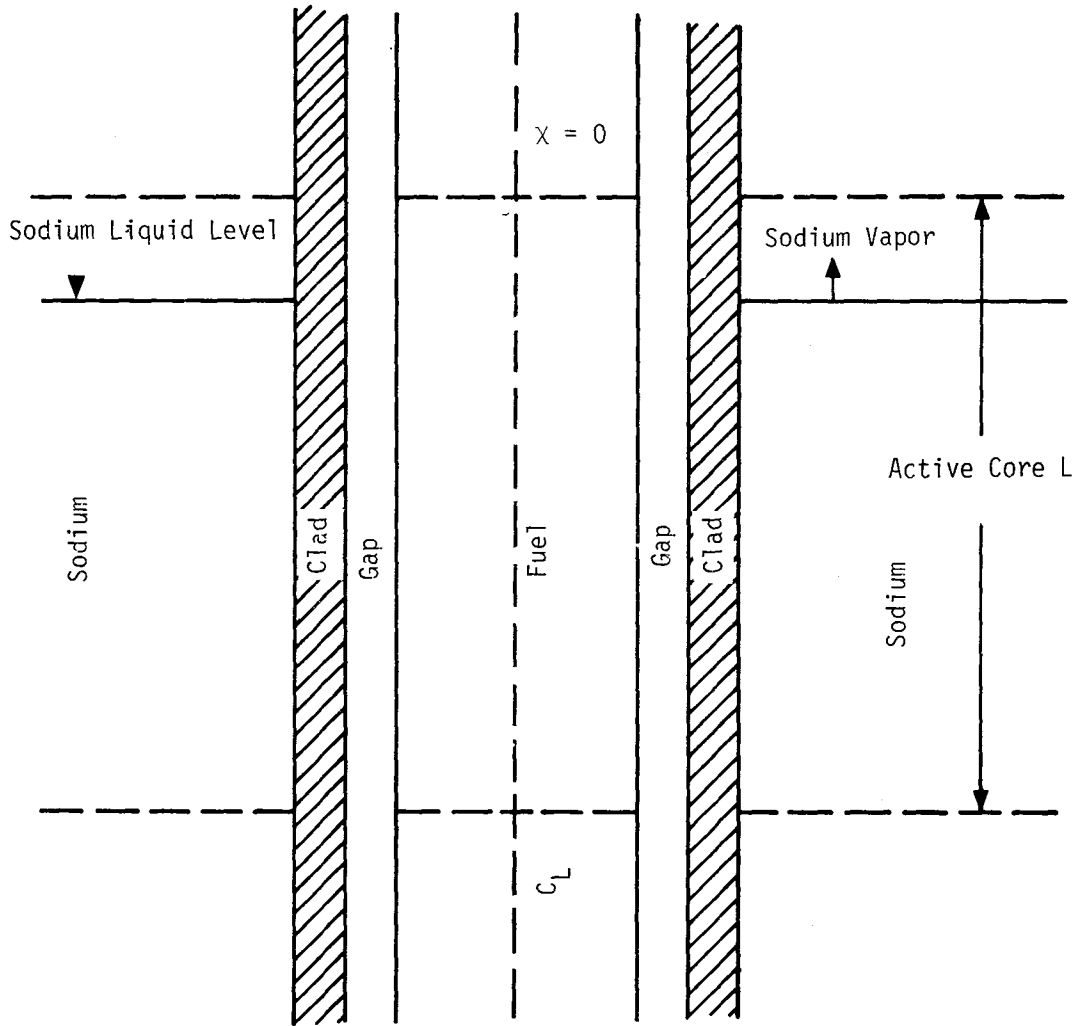


Figure 2.2. Physical Model of the Core Dryout Process.

k_f = thermal conductivity for the fuel

$q'''(x,t)$ = volumetric decay heat

R_1' = thermal resistance
across the gap and the
fuel pellet $= \frac{1}{4\pi k_f} + \frac{1}{h_g P_f}$

where P_f = is the perimeter of the fuel pellet

The cladding temperature distribution is given as

$$(\rho C_p)_\phi \bar{A}_\phi \frac{\partial T_\phi}{\partial t} = k_\phi \bar{A}_\phi \frac{\partial^2 T_\phi}{\partial x^2} + \frac{1}{R_1'} [T_f(x,t) - T_\phi(x,t)] \quad (2.26)$$

$$- \frac{1}{R_2'} [T_\phi(x,t) - T_c(x,t)]$$

where $(\rho C_p)_\phi$ = heat capacity per unit volume of the cladding

k_ϕ = thermal conductivity for the clad

\bar{A}_ϕ = total clad cross-sectional area

R_2' = thermal resistance $= \frac{1}{h_c A_\phi} + \frac{1}{4\pi k_c \ell}$

Both the coolant temperature T_c and the heat transfer coefficient h_c depends on the axial location x . For the vapor region, the temperature is given as

$$(\rho C_p)_v \left[\frac{\partial T_v}{\partial t} + u_v(t) \frac{\partial T_v}{\partial x} \right] = h_v P_\phi [T_\phi(x,t) - T_v(x,t)] \quad (2.27)$$

and the heat transfer coefficient h_v is given by the Bolter-Dittos correlation.

$u_v(t)$ is the vapor velocity and it is determined by the sodium vaporization rate

$$\dot{u}_v(t) = \frac{h_{NB} P_\phi}{\rho_v \bar{A}_{co} h_{fg}} \int_0^{\ell(t)} [T_\phi(x,t) - T_{SAT}] dx \quad (2.28)$$

where $\lambda(t)$ is the location of the liquid-vapor interface. It is related to the receding speed of the sodium level by

$$\lambda(t) = L - \int_0^t u_1(t') dt' \quad (2.29)$$

where

$$u_1(t) = \frac{h_{NB} P_\phi}{\rho_c A_{co} h_{fg}} \int_0^{\lambda(t)} (T_\phi(x,t) - T_{SAT}) dx \quad (2.30)$$

In the lower liquid region, nucleate boiling is assumed to prevail so

$$T_\phi = T_{SAT} \quad \text{for } \lambda(t) > x > 0 \quad (2.31)$$

and the heat transfer coefficient

$$h = h_{NB} \quad \text{for } \lambda(t) > x > 0 \quad (2.32)$$

When the cladding temperature reaches the melting point, equation (2.27) has to be modified to accommodate the phase change. During the melting process, the local clad temperature is constant and is given by

$$T_\phi = T_m \quad (2.33)$$

whereas the amount of clad melt is given by

$$\rho_\phi h_{sf} \frac{dV_m}{dt} = \frac{1}{R_1} (T_f(x,t) - T_m) \quad (2.34)$$

where T_m = melting temperature

h_{sf} = heat of fusion

V_m = amount of clad melt

Failure of the cladding would lead to the release of the fission gas into the sodium stream. As will be shown in Chapter 3, in most cases,

the receding speed of the sodium is fast, therefore, at the start of the melting clad, all the sodium in the core is almost gone. A parametric study is performed to determine the ability of the sodium vapor to disperse the molten clad into the upper core region. The molten droplet size (d) is based on the critical Weber number for atomization, i.e.:

$$\frac{\rho_v (u_v - u_{s.s.})^2 d}{\sigma_{s.s.}} = 12 \quad (2.35)$$

Where

ρ_v = sodium vapor density

u_v = sodium vapor velocity

$u_{s.s.}$ = velocity of molten steel

d = atomization diameter

$\sigma_{s.s.}$ = surface tension of stainless steel

The minimum vapor velocity required to disperse the molten steel is given by [9] :

$$(u_v)_{min} = K \rho_v^{-1/2} \left[g \sigma_{s.s.} (\rho_{s.s.} - \rho_v) \right]^{1/4} \quad (2.36)$$

K is constant depending on the flow regime. It is equal to 0.2 for droplet flow and 1.3 for annular flow.

If the gas velocity is greater than this minimum velocity, the molten steel is assumed to end up in the upper plenum, otherwise, it will move down and plug the flow channel. Eventually, the cladding will be melted. The melting rate can be approximately found by Equation (2.34).

2.5 Subassembly Failure Mode

When the cladding in the core region is melted away, heat can be radiated from the fuel pins to the channel wall. It can be shown in a detailed radiative heat transfer calculation that the inner rows of the fuel pins are heated up adiabatically, while most of the heat incident on the can wall is from the outermost zone (Appendix B). Since the fuel pins are closely packed, the heat up model of the fuel within the sub-assembly can be approximated as a big lump of fuel which radiates heat to the can wall (Figure 2-3). An energy balance of the fuel region gives the temperature rise as:

$$(\rho C_p V)_f \frac{dT_f}{dt} = q'''(t,r) - Q_{RAD} \quad (2.37)$$

where $q'''(t,r)$ is the decay heat and because of the radial power distribution, it is a function of the fuel assembly location.

Q_{RAD} is the total heat radiated from the fuel to the can wall, so the temperature in the can wall is given by

$$(\rho C_p V)_w \frac{dT_w}{dt} = Q_{RAD} \quad (2.38)$$

In determining Q_{RAD} , both the can and the fuel surfaces are assumed to be grey, so

$$Q_{RAD} = A_f \frac{\epsilon_f}{1-\epsilon_f} (\sigma T_f^4 - B_f) \quad (2.39)$$

where ϵ_f is the emissivity of the fuel

B_f is the radiant radiosity from the fuel

A_f is the exposed fuel area

The governing equations for the radiosity are

$$B_f = \epsilon_f \overline{\sigma} T_f^4 + (1 - \epsilon_f) H_f \quad (2.40)$$

$$B_w = \epsilon_w \overline{\sigma} T_w^4 + (1 - \epsilon_w) H_w \quad (2.41)$$

where $H_f = B_w$ (2.42)

$$H_w = B_w F_{w-w} + B_f F_{w-f} \quad (2.43)$$

and

F_{w-w} and F_{w-f} are the view factors for can wall to can wall and can wall to fuel, respectively.

By solving equations (2.37) to (2.43), the time variations of the fuel and the can wall temperatures are determined. If the wall fails before the fuel is melted, collapse of the core is a possible event. In either case, criticality calculation is necessary.

3. RESULTS

The general solution procedure developed in Chapter 2 was used to study characteristics of the sequential events in the CRBRP system in response to the pipe rupture incident. There are at present no data available in the literature for this type of slow decay heat transient.

When the pipe breaks, the sodium inventory in the reactor vessel above the break location is spilled onto the containment floor. The reactor is assumed to be scrammed successfully and the decay heat plus the stored energy are the principal heat sources inside the reactor vessel. The heat generated in the fuel is transferred across the gap to the cladding, and finally, to the sodium liquid. Using the forward march technique, the temperature transients in the fuel, the cladding and the sodium were computed from equations (2.1) - (2.12), and the results are shown in Figure 3.1. The physical parameters for the calculation are tabulated in Tables 3.1 and 3.2.

Using the point model, the average fuel temperature is found to experience a decrease as the power level decays (Figure 3.2). Since the initial fuel temperature profile is parabolic in shape, a more refined heat conduction calculation will give a more accurate transient spatial temperature distribution. The cladding temperature increases to a maximum value of about 1600^oF before it follows the same trend as the fuel temperature. The coolant temperature increases as it absorbs heat from the cladding. In the present calculation, the temperatures of the structures in the upper and the lower plena are assumed to be the same as the coolant temperature. Bubble

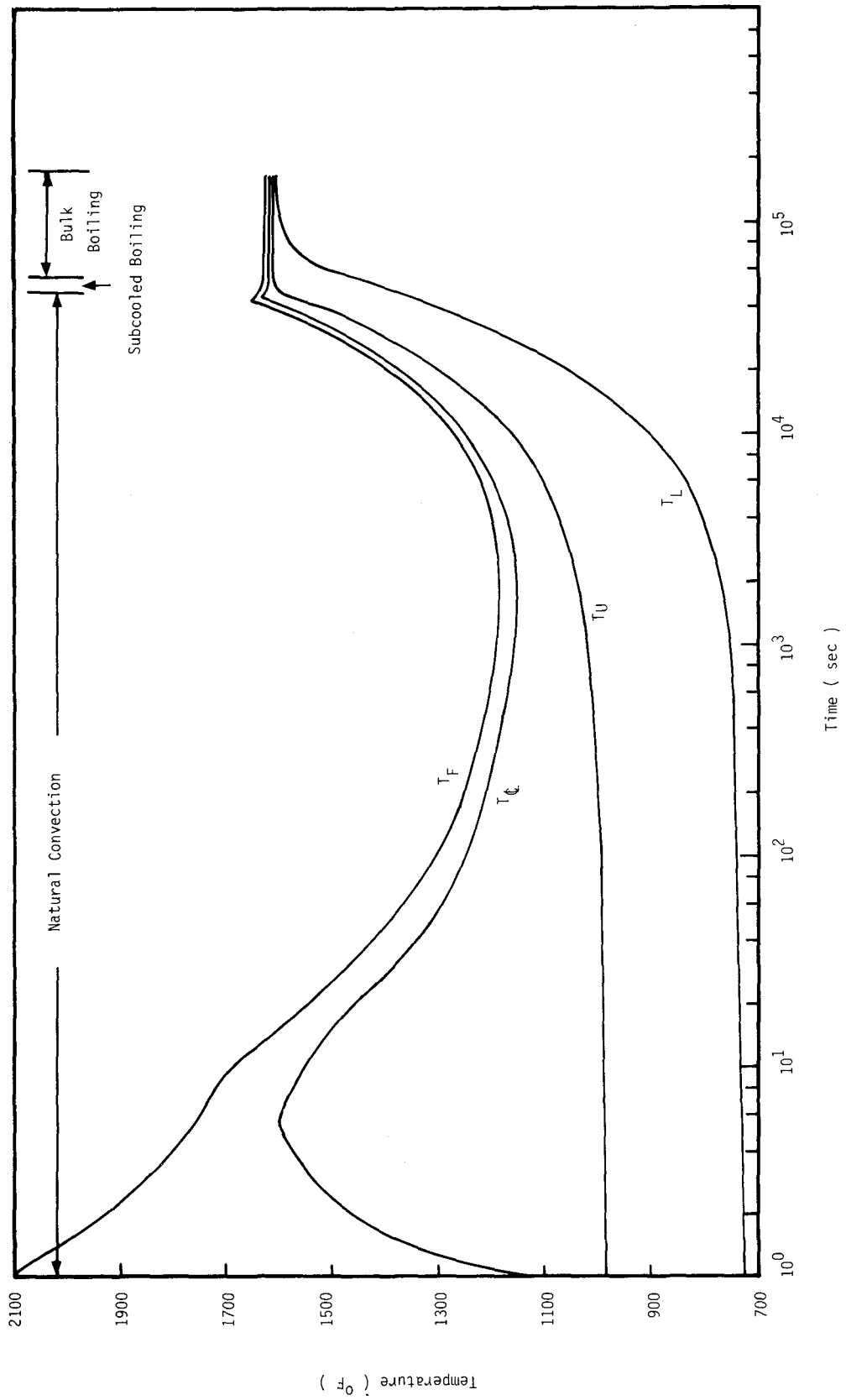


Figure 3.1 Temperature Response during Natural Circulation and Boiling Periods

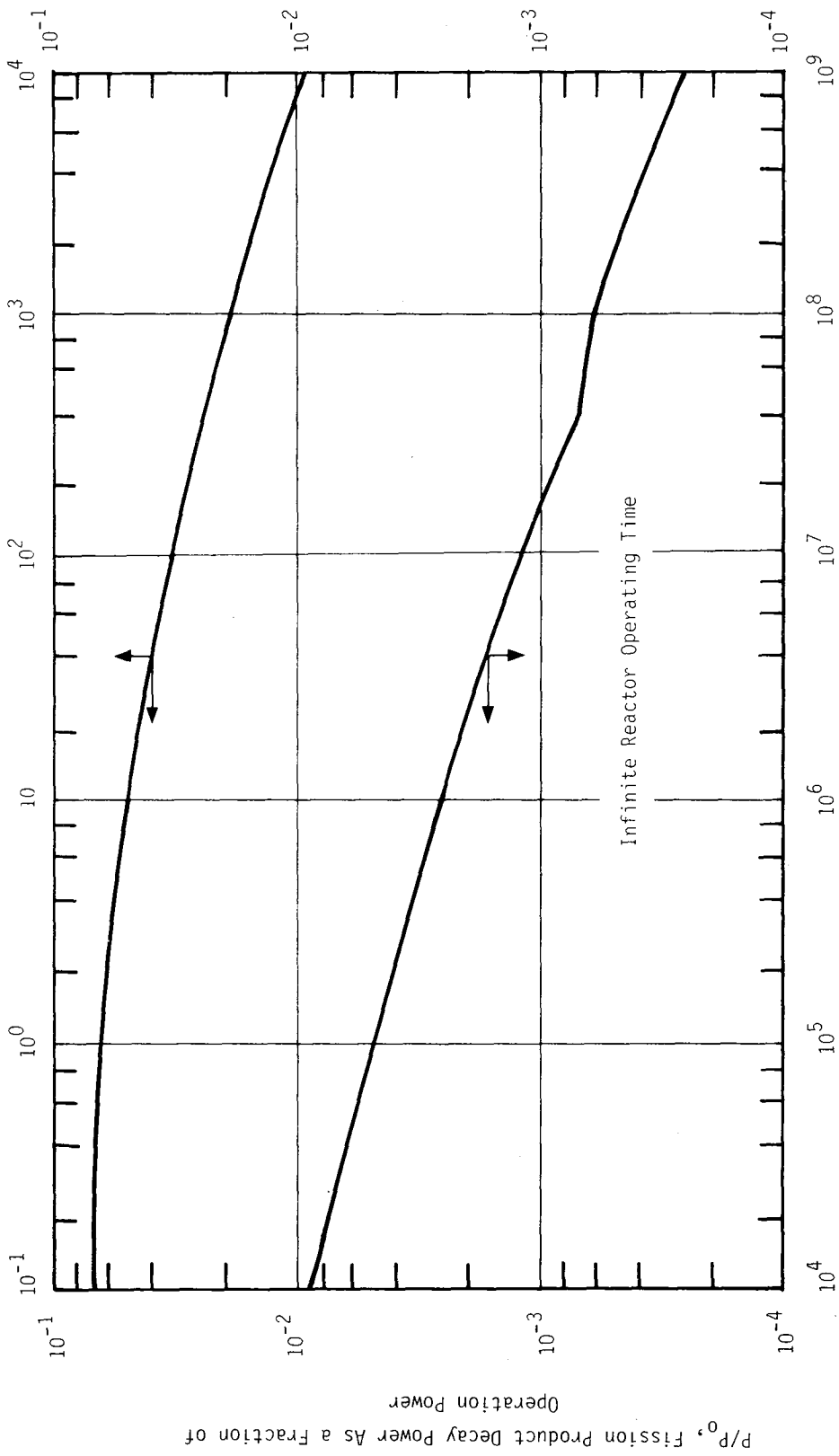


Fig. 3.2 Standard Fission-Product Decay Heat Curve

Table 3.1.

Physical Parameters for CRBR Design.

Coolant Flow Rate	1.15×10^4 lb/sec.
Core Flow Area	9.24 ft ²
Reflector Flow Area	4.2917 ft ²
Average Core Flow Velocity	20 ft/sec.
Inlet Temperature	730 ^o F
Outlet Temperature	995 ^o F
Average Heat Transfer Coefficient	6.05 Btu/ft ² -sec. F
Initial Axial Peaking Factor	1.24
Initial Radial Peaking Factor	1.20
Mass of Fuel	14, 486 lb
Mass of Cladding	33, 963 lb
Mass of Sodium	5.3017×10^5 lb
<u>VESSEL PARAMETERS</u>	
Liquid Volume of Upper Plenum	6607 ft ³
Liquid Volume of Inlet Plenum	3218 ft ³
Liquid Volume of Core	27.72 ft ³
External Surface Area	2600 ft ²
<u>FUEL ASSEMBLIES</u>	
Maximum Midwall Cladding Temperature	1350 ^o F
Maximum Assembly Mixed Mean Outlet Temp.	1107 ^o F
Maximum Fuel Centerline Temp.	4780 ^o F
Average Linear Power	6.6 KW/ft
Peak Linear Power	11.1 KW/ft
Maximum Linear Power	14.4 KW/ft

Table 3.1. (Continued)

Maximum Fission Gas Pressure	186 psia
Maximum Assembly ΔP	111 psia
<u>CRBRP FUEL ASSEMBLY DETAILS</u>	
Rods per assembly	217
Rods (total number)	42,966
Rod outside diameter	0.230 in
Rod radial spacing	0.056 inch wire wrapped around fuel rod cladding in clockwise helical spiral with pitch of 11.9 inch
Rod triangular pitch	0.2877 in
Hydraulic Diameter	0.0139 ft
Clearance between fuel rod assemblies at wires	0.017 in
Clearance between fuel rods	0.0577 in
Cladding thickness	0.015 in
Rod axial support	17 key shaped rails through keyhole slots in bottom end caps
Rod length	114.40 in
Pellet Column Length	64 in including two 14 inch axial blankets
Fission Gas Plenum Length	48.0 in
Fission Gas Plenum Available Volume-Cold	1.274 in ³
Lower axial blanket length	14 in
Lower axial blanket composition	Depleted uranium oxide
Core region length	36 in
Core Pellet Material	Plutonium-uranium oxide
Core pellet Diameter	0.1935 in

Table 3.1. (Continued)

Pellet Length	0.205 to 0.283 in
Density:	
Nominal (percent of theoretical)	91.3
Cold smeared(percent of theoretical)	85.5
Plutonium Content:	
Inner enrichment zone (weight percent)	18.7
Outer enrichment zone (weight percent)	27.1
Ratio outer/inner zone	1.45
Diametral gap between fuel cladding and fuel pellet	0.0065 in
Upper axial blanket length	14 in
Upper axial blanket composition	Depleted uranium oxide
Axial Blanket Pellet	0.1935 in
Axial blanket pellet length	0.31 to 0.46 in
Nominal density (percent of theoretical)	97.1
Diametral gap between fuel cladding and axial blanket pellets	0.0065 in
Inlet Nozzle Discrimination Post Max. Dia.	1.750 in
<u>NOMINAL RADIAL BLANKET ASSEMBLY DESIGN PARAMETERS</u>	
Assemblies (number)	150
Blanket Rods per Assembly (number)	61
Number of Flow Orificing Zones	4
Pitch to Diameter Ratio	1.077
Blanket Rod Spacing	Wire-Wrap, 0.037" dia. wire with 4" pitch
Blanket Rod Length	105 in
Cladding and Duct Material	20 percent cold worked Type 316 Stainless Steel

Table 3.1. (Continued)

Rod Outside Diameter	0.520 in
Cladding Thickness	0.015 in
Fuel Pellet Column, inch (uranium-dioxide)	64
Pellet Diameter	0.485 in
Pellet Length,	0.5 in
Pellet Density, % theoretical	95.6
Smear Density, % theoretical	93.7
Pellet Material	Depleted UO ₂
Diametral Gap between Cladding and Pellet (initial, cold), inch	0.005 in
Distance across Flats on Duct Inside	4.450
Duct Wall Thickness,	0.100
Number of Radial Blanket Rows	2-1/2
Fuel Arrangement	Column of Cylindrical Pellets
Fission Gas ₃ Cold Available Plenum Volume, in ³	5.93
Fill Gas	He
Fill Gas Pressure, atm (at ambient temp.)	1
Spacer Material	316 SS - 17% CW
Assembly Pitch	4.760 in

Table 3.2 Thermophysical Properties of Materials

	Temperature (° C)									
	25	500	1000	1500	2000	2500	3000			
Fuel ($U_{0.8}P_{0.2}O_2$)										
Melting Point (3150°C)										
K_f (cal/sec-cm c)	0.015	0.009	0.006	0.005	0.005	0.06	0.007			
ρ_f (gm/cm ³)	11	10.4	10.2	10.0	9.9	9.8	8.4			
C_{pf} (cal/gm c)	0.058	0.074	0.078	0.085	0.10	0.13	0.12			
Cladding (Stainless Steel)										
Melting Point (2800°C)										
k_ϕ (cal/sec-cm C)	.04	.05	.07							
ρ_ϕ (gm/cm ³)	8.0	7.7	7.5							
$C_{p\phi}$ (cal/gm C)	0.11	0.14	0.16							
Coolant (Sodium) Temperatures(°C)										
Boiling Point (883°C)										
k_c (cal/sec cm C)	.20	.19	.18	.17	.16	.15	.14	.13	.12	.11
ρ_c (gm/cm ³)	.93	.90	.88	.86	.83	.81	.79	.77	.74	.71
C_{pc} (cal/gm C)	.33	.32	.31	.31	.31	.30	.30	.30	.31	.32

nucleation is started when the cladding reaches the incipient boiling temperature of 1640⁰ F.

When bubbles are nucleated, the heat transfer at the clad surface is improved. Both the fuel and the clad experience a temperature drop before they reach a quasi-steady state temperature during nucleate boiling.

The heat transfer coefficient and the circulation rate during the natural circulation period are shown in Figure 3.3. The natural circulation rate through the core is about 1/250 of the normal force convection rate. In the actual system, since force flow is maintained when the pipe ruptures, there is a finite time for the coolant to coast down to the natural convection range. This finite time is conservatively neglected in the present analysis. On the other hand, the time delay required for the scrambling is also neglected. As the circulation rate decreases, the coefficient decreases, but increases as boiling starts. As reflected in Figure 3.1, the fuel and the cladding temperatures remain fairly close to the saturation temperature during boiling. It takes 5 hours to heat up the cladding to the recipient boiling temperature; 2 more hours to start bulk boiling, and 32 hours for complete boiling off of the sodium in the upper plenum.

A simple heat balance table for the transient is shown in Table 3.3. This table serves the purpose of a quick check of the heat transfer calculation. It is observed that the sodium and the steel structures serve as the major heat sinks for the decay heat generated in the core where the heat loss from the vessel surface is negligible.

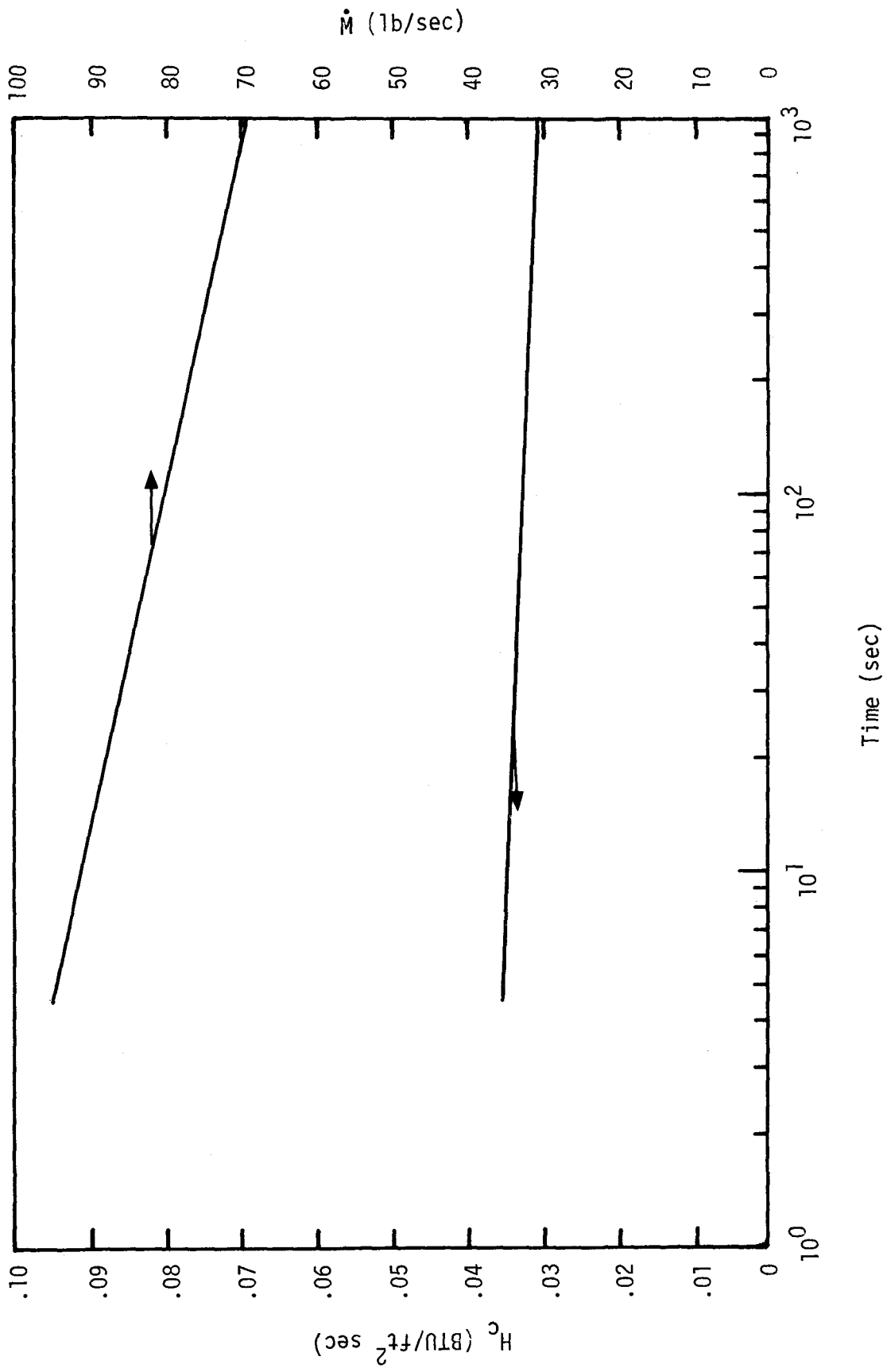


Fig. 3.3 Heat Transfer Coefficient and Circulation Rate

Period	Time (hr)	Heat Generated in the Fuel (Btu)	Heat Content in the Fuel (Btu)	Heat Content in the Cladding (Btu)	Heat Content in the Sodium (Btu)	Heat Content in Structural Material (Btu)
Natural Convection	5.62	2.08×10^8	-5.36×10^5	2.56×10^5	8.31×10^7	9.36×10^7
Subcooled Boiling	1.15	2.93×10^7	-1.86×10^4	-7.43×10^3	9.8×10^6	10.8×10^6
Nucleate Boiling	32	5.9×10^8	-6.71×10^3	-420.8	5.75×10^8 (vaporize)	0

Table 3.3.

Heat Balance Table.

Because of the low flow rate, the pressure drop across the core is about 0.01 psi during the natural circulation period. The pressure drop is increased by a factor of 3 during the two-phase bubbling flow.

As the sodium level recedes during the core dryout period, the upper part of the cladding could only be cooled by the sodium vapor which is much less effective than by nucleate boiling. In fact, the clad heats up almost adiabatically where there is no sodium as evidenced from the calculational result shown in Fig. 3.4. The same observation can be applied to the fuel temperature. If an axial power distribution as shown in Fig. 3.5 is used in the heat calculation, the melting will occur at a location of 0.006 ft, below the top of the active core. The melting rate is estimated to be $0.08 \text{ ft}^3/\text{sec}$. It is found that at the sodium vapor velocity the molten steel cannot be atomized. In accordance to equation 2.36, the sodium vapor velocity is not high enough to carry the molten steel to the upper blanket region. This leads to the expectation of the downward motion of the molten cladding steel. Lower blanket flow blockage is expected.

The receding speed of the sodium level is shown in Fig. 3.5. As the sodium level moves downward, less vapor is generated, so both the vapor velocity and the vapor heat transfer coefficient decreases (Figs. 3.5 and 3.6).

It is found that the axial conduction has minor effects on mitigating the temperature rise at the hot spot. The temperature rises almost linearly in the fuel and in the cladding, once dryout occurs. When clad melting starts, the sodium level recedes to a level which is 1 ft from the bottom of the active core. In view of the low heat transfer

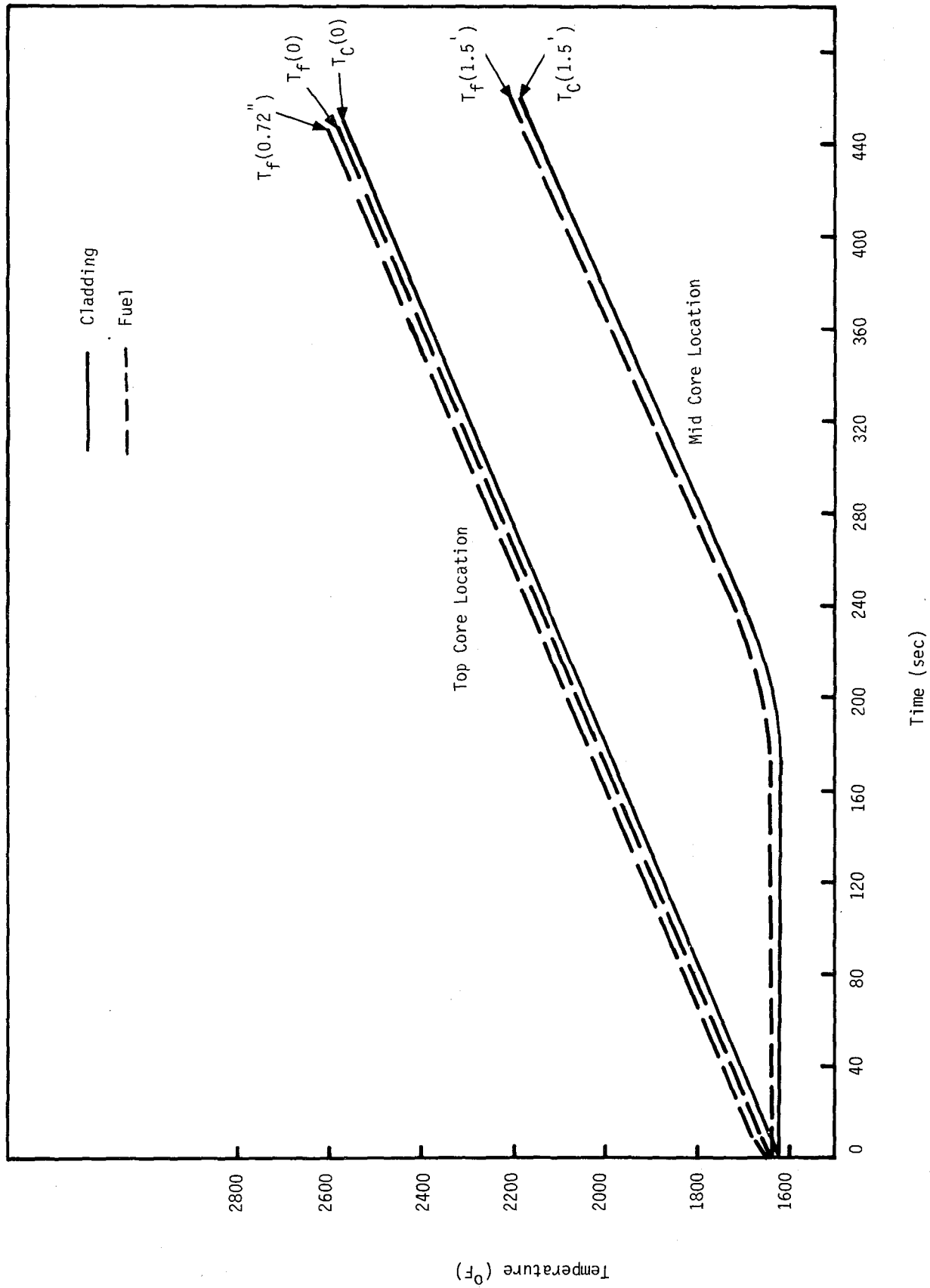


Figure 3.4 Axial Cladding and Fuel Temperatures During Core Dryout

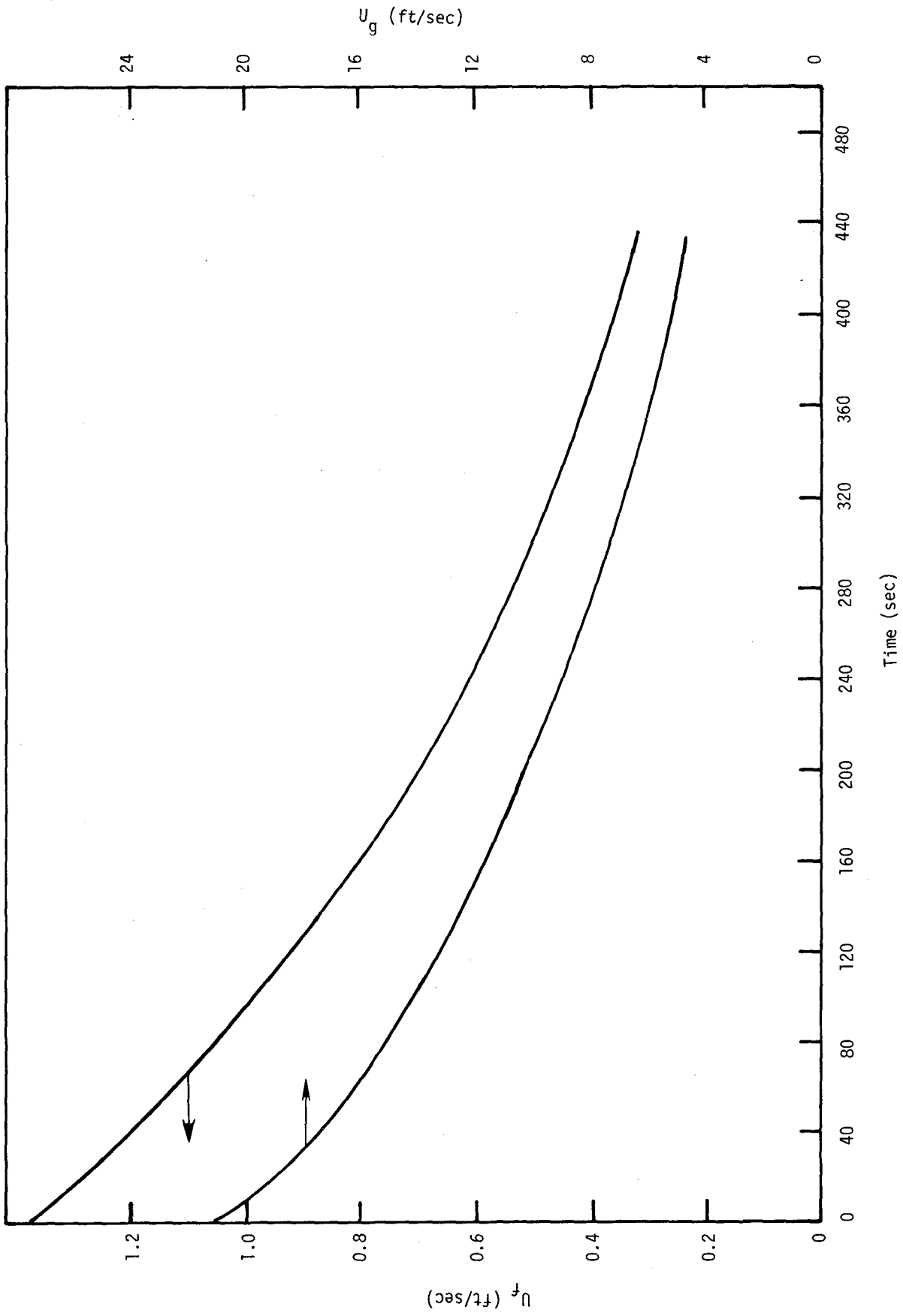


Fig. 3.5 Receding Speed of Liquid Sodium (U_f) and Sodium Vapor Velocity (U_g)

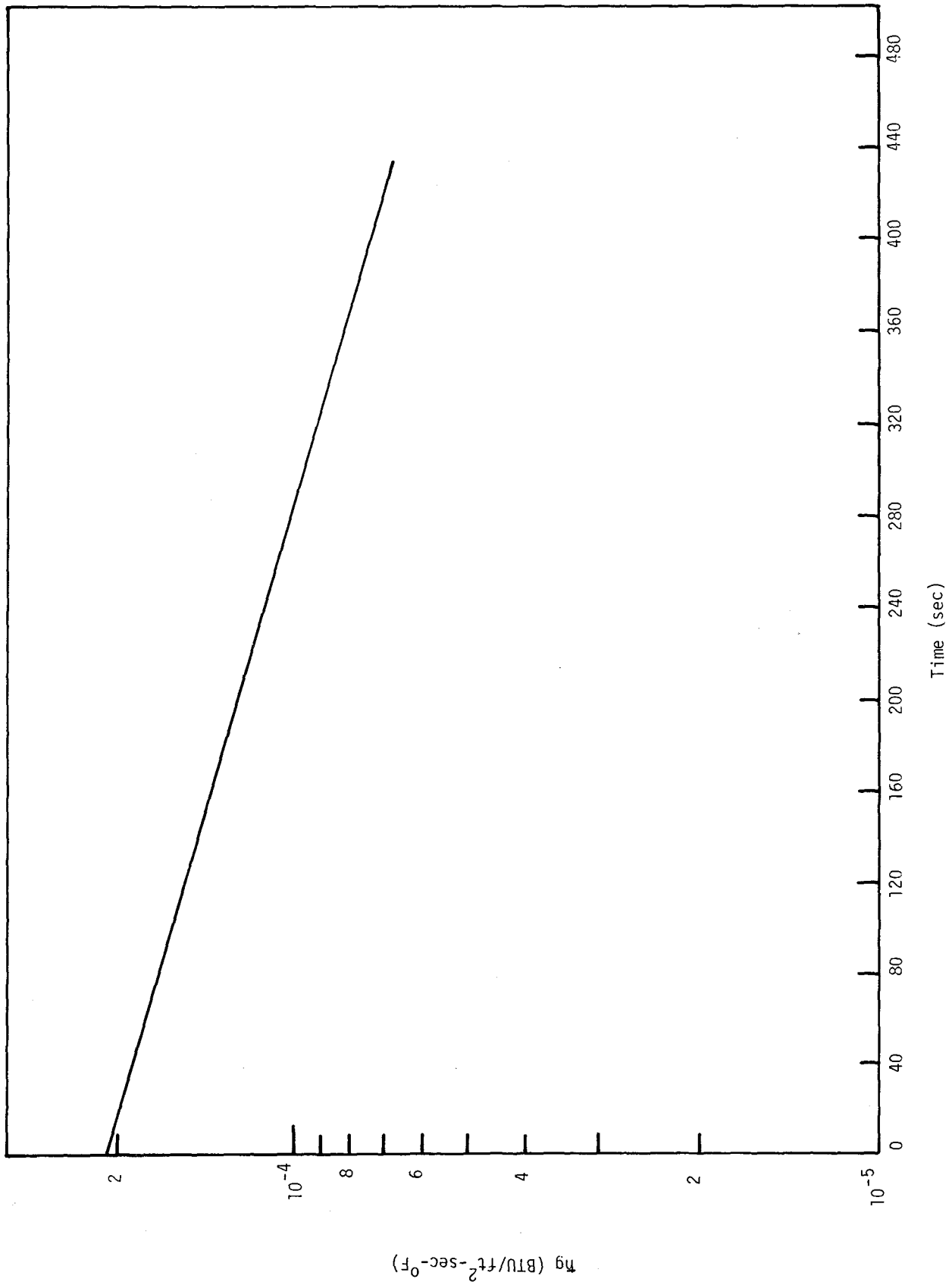


Fig. 3.6 Sodium Vapor Heat Transfer Coefficient

coefficient, the gross clad melting is estimated by an adiabatic model. It is found that the time for all the clad to melt is 83 sec. At that time, the fuel temperature is 2823⁰ F.

The loss of cladding integrity leads to the release of the fission gas. Since the release process is rather spontaneous, the effect of fission gas release is not modeled in this preliminary study.

The loss of both cladding and sodium in the core region would lead to reactivity insertion. However, with the control rods inserted, this positive reactivity effect is not large enough to overcome the negative reactivity effect of the control rods. The reactor remains subcritical until fuel movement occurs.

The complete melting of all the cladding takes place in about 83 sec, whereas melting of the fuel would start in 25 min from an initial temperature of 2823⁰ F, if it is heated up adiabatically. It is conceivable that small portions of the fuel may experience melting before all the cladding disappears from the core region. But, because of the current design of the fuel rod (Figure 3.7), the loss of the cladding might not cause any major fuel dislocation if the fuel pellets are fused together.

During the clad melting, the bare fuel rods radiate heat to the can wall. Using the calculational model outlined in Chapter 2, the can wall fails in 50 sec. Once the can fails, the fuel rod loses its supporting structure (Figure 3.8). It is probable that the fuel rods will collapse into a pile of pellets before pellet melting occurs. Some relevant properties and criteria for the stainless steel and the fuel pellets are tabulated in Table 3.4.

Four cases of recritical calculations for the fuel pellets were performed. In all of these cases, the pile is assumed to be cylindrical

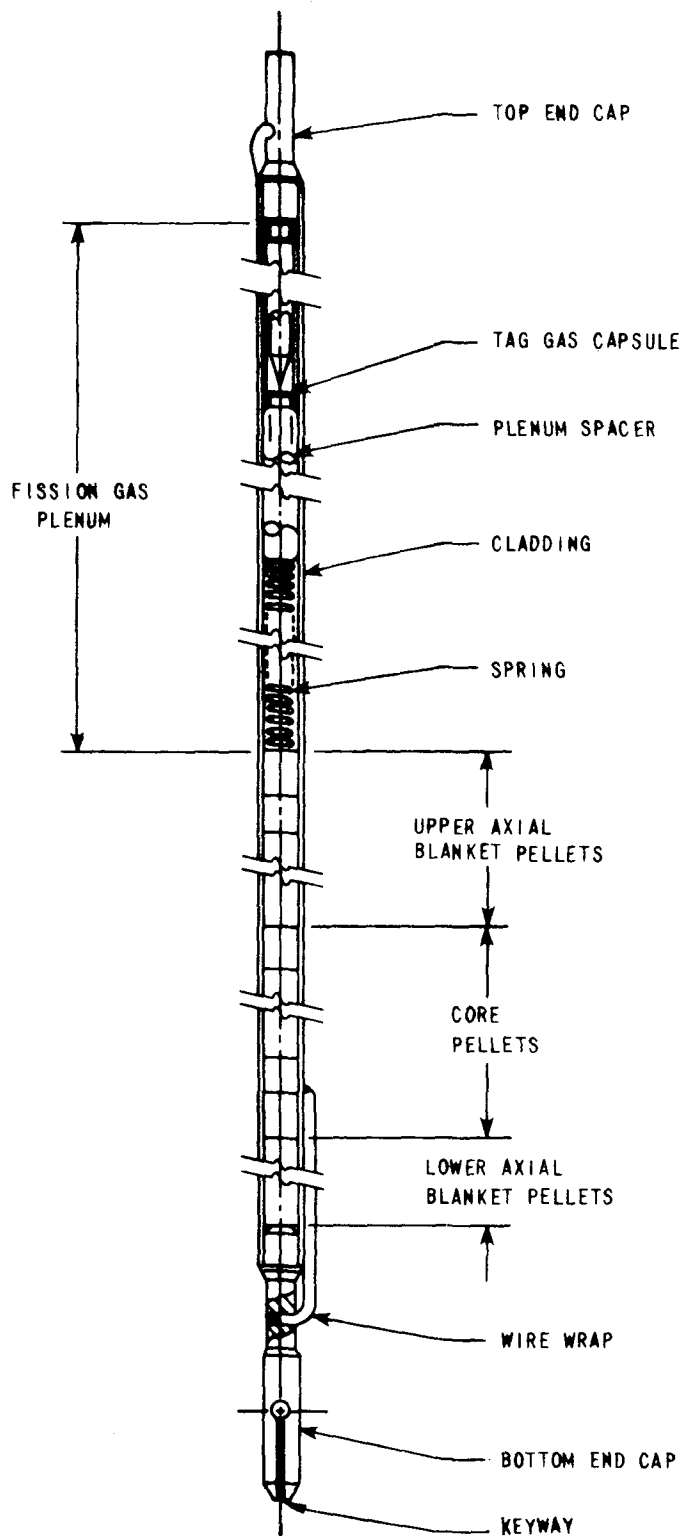


Figure 3.7 Fuel Rod Schematic for CRBRP Design

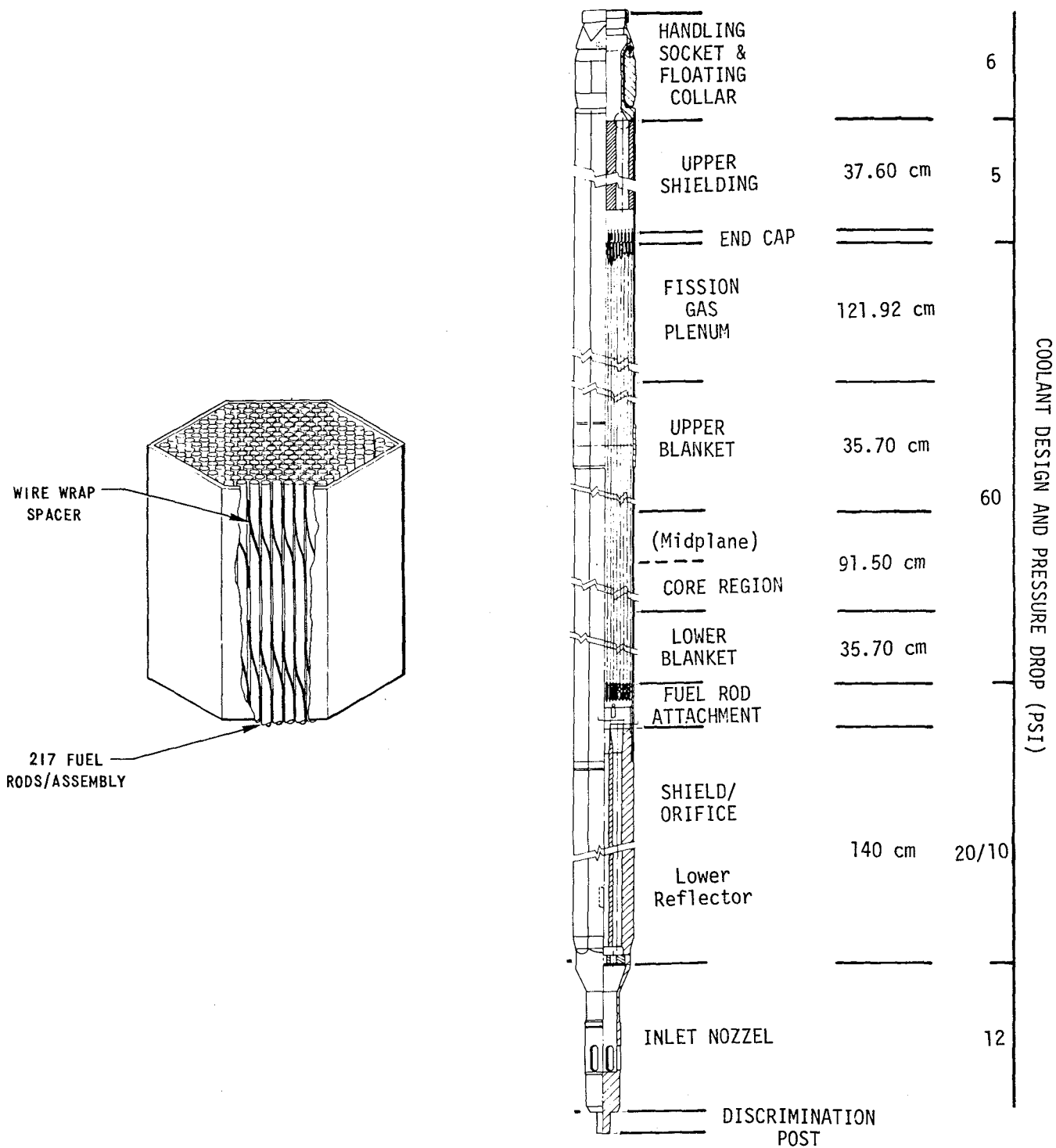


Fig. 3.8 Fuel Assembly Schematic for CRBRP Design

	Fuel	Cladding
Material	$(\text{Pu}_{0.2}\text{U}_{0.8})\text{O}_2$	Stainless steel type 316
Melting Temperature	5,018° F (2,770° C)	2,570° F (1,410° C)
Yield Point (below 3,000° F)	1.1549×10^4 (psi) $(0.796 \times 10^8 \text{ (N/m}^2\text{)})$	23,000 (psi) $(1.5858 \times 10^4 \text{ (N/m}^2\text{)})$

Table 3.4.

Properties of Fuel and Cladding Materials.

in shape. The lower boundary is stainless steel while the upper boundary can be vacuum or stainless steel. Two void fractions were chosen for the calculation, namely 30% and 50%. For both cases, if no control rod material is assumed in the fuel region, the reactor will go critical. If control rod material is homogenously mixed with the fuel pellet, the reactor will be in a subcritical state. These results are summarized in Table 3.5.

Cases	Boundary Condition	Void Fraction	k_{eff}
1	No stainless at top boundary	30%	1.000324
2	Stainless steel at top and bottom boundaries	30%	1.2284
3	Stainless steel at top and bottom boundaries	50%	1.11427
4	Homogenous mixture of fuel and control rod material		subcritical

Table 3.5.
Results of Recritical Calculation.

4. CONCLUDING REMARKS

The postulated accident involving sudden rupture of all pipes connected to the reactor vessel (with scram) is well-defined mathematically, and hence was chosen as possibly representative of a class of accidents in which both some primary system piping rupture and a loss of heat removal capability from the reactor vessel result. Of first interest was a determination of the rough time scale to sodium boiling, clad melting and possible core collapse, since many of the consequent phenomena depend on the then-current decay heat rate.

Modeling the various possible phenomena which might be important in subsequent motion of the fuel, remains to be done as a follow-on study. The role of gravity as affected by core support structure and upper blanket and plenum structure remains to be examined. The behavior of irradiated fuel pellets under relatively slow heating rates prior to melting remains to be studied. The possible re-configurations of the core remain to be estimated. And the applicability of current ideas on core boilup and dispersion remains to be investigated.

All this study does is provide a possible starting point for further studies of a rather different class of core disruptive accidents than the currently emphasized unprotected loss-of-flow and transient overpower accidents.

While no attempt has been made herein to identify specific initiators which might lead to a situation equivalent to that postulated, severe earthquakes certainly provide one possible source.

5. REFERENCES

1. Fauske, H. K., "Boiling Flow Regime Maps in LMFBR HCDA Analysis," ANS Transactions, Vol. 22, p. 385, November 1975
2. Hakim, S. J., and R. J. Henninger, "TRANSIT: A Computer Code for a Mechanistic Analysis of the Transition Phase of an FBR Accident," ANS Transactions, Vol. 24, p. 261, November 1976.
3. Catton, I., and V. K. Dhir, "Post-Accident Heat Removal for LMFBRs," University of California, Los Angeles, UCLA-ENG-7593, November 1975.
4. Amorose, A., et al., "An Overview of Pool-Type LMFBRs," ANL Report, January 1976.
5. WADCO Corp., "Preliminary Safety Analysis of the Fast Flux Test Facility," Vols. 1 and 2, September 1970.
6. Project Management Corporation, "Preliminary Safety Analysis of the Clinch River Breeder Reactor," June 1976.
7. Dulton, J. D., and J. R. Welty, "An Experimental Study of Low Prandtl Number Natural Convection in an Array of Uniformly Heated Vertical Cylinders, J. of Heat Transfer, Vol. 97, p. 372-377, August 1975.
8. Collier, J. G., Convective Boiling and Condensation, McGraw-Hill, New York, 1972.
9. Wallis, G. B., One-Dimensional Two-Phase Flow, McGraw-Hill, New York, 1969.
10. Reilly, J. T., Radiative Transfer within a Fast Reactor Subassembly, M. S. in Engineering, University of California at Los Angeles, 1977.

APPENDIX A

POST ACCIDENT FLOW RATES

Coolant flow rates during the post-accident period have a significant bearing on assessment of heat removal. For the CRBR design, a hydraulic model of coolant flow can be established, as shown in Figure A.1. The model assumes that the flows are in quasi-steady state, and that each individual flow rate, \dot{M}_j , within the reactor vessel, is related to the corresponding pressure drop, ΔP_j , as follows:

$$\Delta P_j = K_j \frac{\dot{M}_j^2}{2g\rho_c}, \quad (\text{A.1})$$

where K_j are the values of the flow constants given in Figure A.1. Since the resistance in the leakage flow region is large in comparison with the other regions in parallel, the leakage flow can be neglected. During the natural circulation, the flow path can be simplified as a single circuit, as shown in Figure A.2. This may be an oversimplified picture of the flow paths, but is adopted here as a first order of estimation of the post accident flow rate.

The heating of the sodium in the core provides the available pressure for the natural circulation. The pressure developed is approximated as

$$\Delta P = \rho_c \beta (T_o - T_i) L, \quad (\text{A.2})$$

where

g = acceleration due to gravity

ρ_c = sodium density

β = coefficient of expansion

T_o = temperature of sodium at outlet of the core

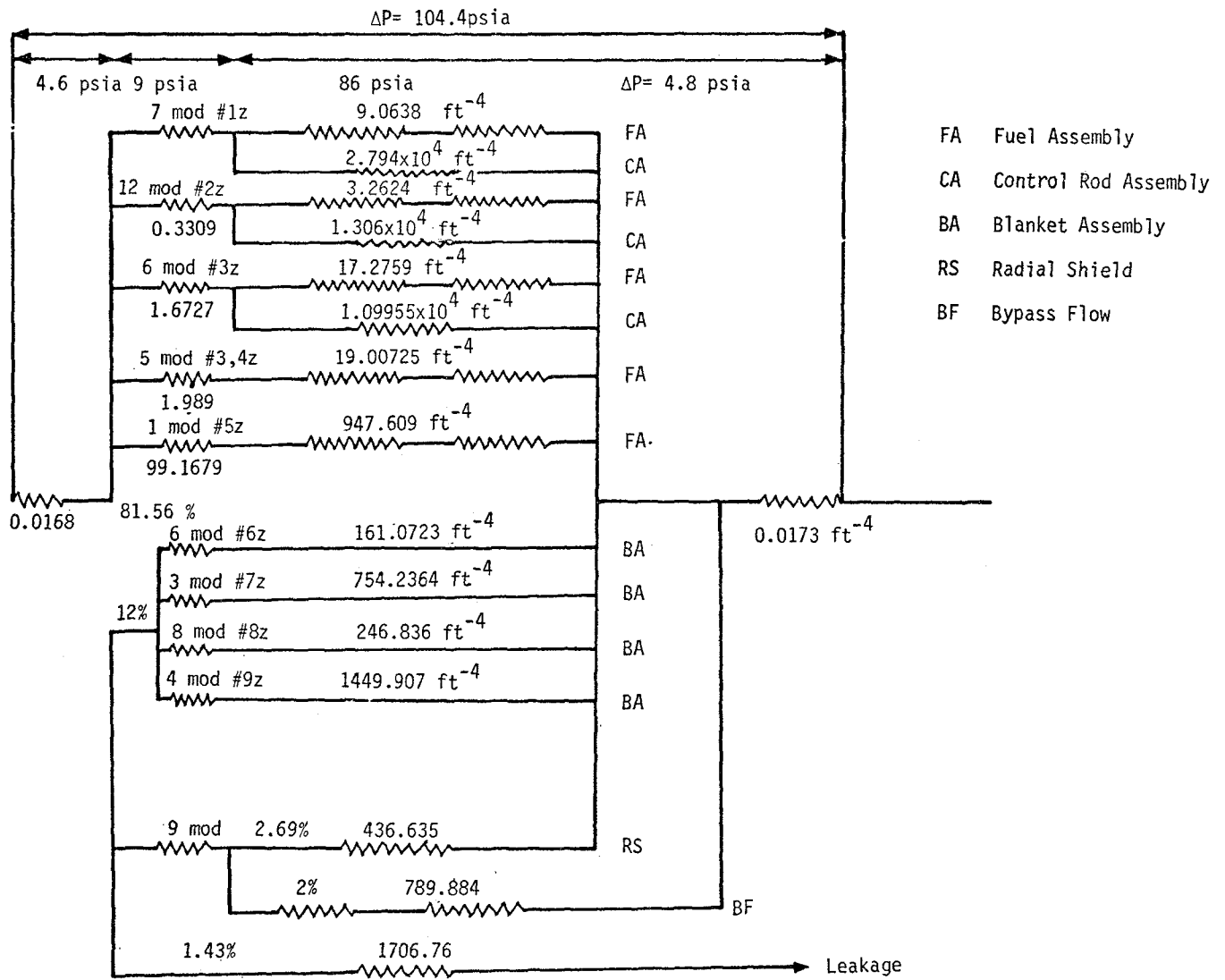


Figure A.1 Hydraulic Flow Resistance Circuit Diagram

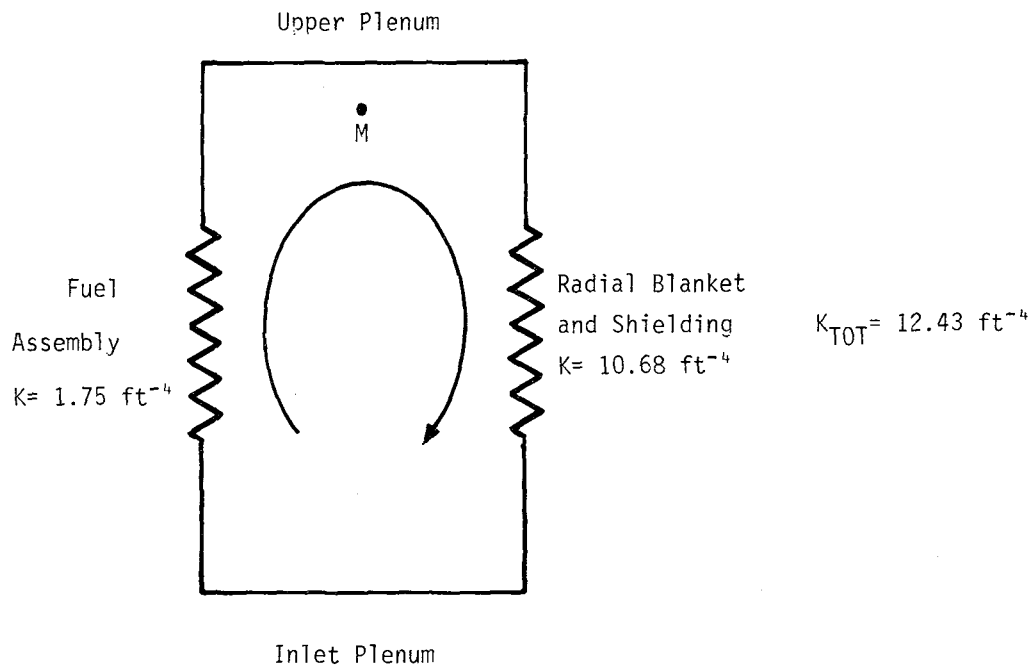


Figure A.2. Simplified Hydraulic Circuit for Natural Convection.

T_i = temperature of sodium at inlet of the core

L = distance between inlet and outlet.

If the flow circuit is quasi-steady, then the pressure available must be equal to the pressure loss throughout the circuit, i.e.

$$\Delta P = K_{TOT} \frac{\dot{M}_j^2}{2g\rho_c}, \quad (A.3)$$

where K_{TOT} is the total flow resistance.

Since the temperature difference ($T_o - T_i$) can be related to the cladding temperature as

$$\dot{M}_c C_{pc} (T_o - T_i) = h_c A_\phi (T_\phi - T_c), \quad (A.4)$$

by combining (A.2), (A.3) and (A.4), we obtain the quasi-steady circulation rate as

$$B_1 \dot{M}^3 + B_2 \dot{M}^2 - B_3 = 0 \quad (A.5)$$

where

$$B_1 = 2C_{pc} K_{TOT} \quad (A.6)$$

$$B_2 = h_c A_\phi K_{TOT} \quad (A.7)$$

$$B_3 = 4\beta h_c A_\phi (T_\phi - T_i) \rho_c^2 g L. \quad (A.8)$$

APPENDIX B

THERMAL RADIATION EFFECTS ON SUBASSEMBLY WALL FAILURE

In the detailed radiative heat transfer calculation, the fuel pins within the subassembly are divided into semitransparent circular rings. A set of linear, non-homogenous equations [10] describes the incident thermal flux on each surface of these rings. Using the Monte Carlo method, the macroscopic radiative properties within the unit cell such as transmittance, reflectance and absorptance can be determined. The average temperature of each segment and the can wall is then calculated from a simple energy balance in which azimuthal conduction is neglected.

Figure B.1 shows the temperature rise rate for each row within the array. Comparing with the rate of increase, under adiabatic conditions, only the two outermost rows are affected by the can wall temperature. At the time of wall failure, temperature differences of 80° C were calculated on the outside row of pins. This temperature difference leads to the possibility of pin failure via a thermal stress mechanism.

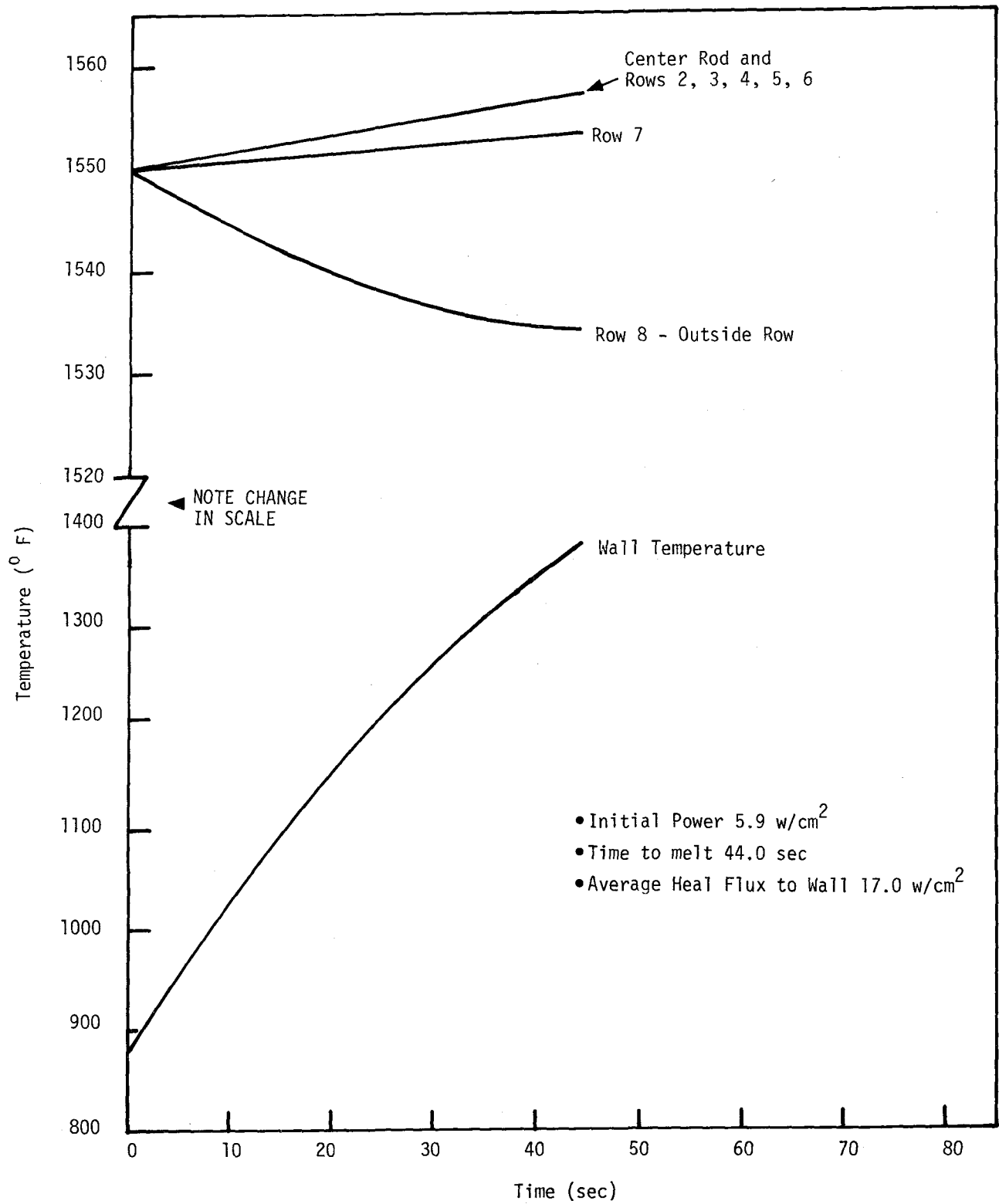


Fig. B.1 Average Fuel Pin Temperatures after Clad Melt